THE JOURNAL OF BIOLOGICAL CHEMISTRY
Vol. 279, No. 8, Issue of February 20, pp. 7159–7168, 2004

Printed in U.S.A.

The Three-dimensional Structure of the Cardiac L-type Voltage-gated Calcium Channel

COMPARISON WITH THE SKELETAL MUSCLE FORM REVEALS A COMMON ARCHITECTURAL MOTIF*

Received for publication, July 24, 2003, and in revised form, November 19, 2003
Published, JBC Papers in Press, November 22, 2003, DOI 10.1074/jbc.M308057200

Ming-Chuan Wang‡, Richard F. Collins‡, Robert C. Ford‡, Nicholas S. Berrow§, Annette C. Dolphin§, and Ashraf Kitmitto‡¶

From the ‡Department of Biomolecular Sciences, University of Manchester Institute of Science and Technology, Manchester M60 1QD and the §Department of Pharmacology, University College London, Gower St., London WC1E 6BT, United Kingdom

We describe here the first three-dimensional structure of the cardiac L-type voltage-gated calcium channel (VGCC) purified from bovine heart. The structure was determined by electron microscopy and single particle analysis of negatively stained complexes, using the angular reconstitution method. The cardiac VGCC can be isolated as a stable dimer, as reported previously for the skeletal muscle VGCC, with a central aqueous chamber formed by the two halves of the complex. Moreover, we demonstrate that the dimeric cardiac VGCC binds the dihydropyridine [^{3}H]azidopine with a K_d ~310 pM. We have compared the cardiac VGCC structure with the skeletal muscle form, determined using the same reconstructive methodology, allowing us to identify common and distinct features of the complexes. By using antibody and lectin-gold labeling, we have localized the intracellular β polypeptides and the extracellular glycosylation sites of the skeletal muscle VGCC, which can be correlated to the cardiac three-dimensional structure. From the data presented here the assignment of the orientation of the VGCC complexes with respect to the lipid bilayer is now possible. A difference between the cardiac and skeletal muscle ion channels is apparent in the putative transmembrane region, which would be consistent with the absence of the γ subunit in the cardiac VGCC assembly.

In the heart, L-type voltage-gated calcium channels (VGCCs)[1] are essential for regulating the influx of Ca^{2+} ions across the sarcolemmal membranes, which are essential for muscle contraction. The blockade of Ca^{2+} entry through the cardiac VGCC represents one of the principal approaches for the treatment of ischemic heart disease. The VGCCs are often referred to as dihydropyridine receptors due to the high affinity binding of the dihydropyridine group of agonist and antagonist drugs. The calcium-conducting pathway of the VGCCs is formed by the α1 polypeptide, and 10 different tissue-specific isoforms of the α1 subunit have been identified to date (α1A–α1I, α1S, now termed $Ca_v1.1$–$Ca_v3.3$). Common to all of the α1 isoforms is a transmembrane domain composed of four homologous repeats each containing six α-helices (1). The symmetrical arrangement of the S6 and S5 helices together with the linker polypeptide, contributed from each transmembrane segment, is believed to form the ion channel pore (2). The α1C ($Ca_v1.2$, ~240 kDa) is enriched in mammalian heart and vascular smooth muscle, whereas α1S ($Ca_v1.1$, ~175 kDa) is expressed in skeletal muscle (1). There is a 66% sequence homology between these two α1 isoforms with conservation of the transmembrane repeats and the III–IV loop. Differences arise in the N- and C-terminal domains, which are slightly larger in the α1C polypeptide. In addition, regions assigned to the cytoplasmic side of the membrane are less well conserved (3). The α1 polypeptides of the VGCCs are stoichiometrically associated with a variable number of accessory subunits (4). In the heart, two additional proteins, α2δ and β, are believed to form the cardiac VGCC by non-covalent association with the α1C subunit (for review see Ref. 5). A diversity of α2δ subunits has been reported, and to date four genes have been identified with type 1 and, to a much lower extent, with α2δ-3 found in the heart (6). The α2 polypeptide is entirely extracellular, heavily glycosylated, and is anchored to the membrane via disulfide bonding to the δ polypeptide (7, 8). Four β isoforms have been identified (β_1–β_4), with β_2 (~66 kDa) found in high density in the heart together with β_{1b} and, depending on species, β_3 (9), with β_{1a} (~54 kDa) specific to skeletal muscle (10). An additional γ polypeptide (~30 kDa) completes the fully assembled skeletal muscle VGCC, with topology studies indicating that it is predominantly hydrophobic with four transmembrane α-helices (11). Although neuronal isoforms of this subunit have been identified (12), there is no direct evidence for the presence of a γ subunit forming part of the cardiac ion channel. The functions of these auxiliary subunits have not been fully established, but involvement in channel gating, stabilization of ligand binding, and the correct plasma membrane trafficking of the α1 polypeptide have been suggested (13–17).

We have reported previously the three-dimensional structure of dimeric VGCC complexes, purified from rabbit skeletal muscle. The structure was derived from negatively stained (uranyl acetate) complexes using the random conical tilt method (18) with an estimated resolution of 2.7 nm (19). Biochemical and structural data indicated that the VGCC complexes were dimeric. This dimer was roughly toroidal in shape, ~21 nm across, and composed of two arch-shaped monomers each ~7.5 nm thick. The two arches contact at each end creating a central void (~8 nm in diameter) that is isolated from the

* This work was supported by the British Heart Foundation via a Basic Science Lectureship Award BS/97002 (to A. K.). The costs of publication of this article were defrayed in part by the payment of page charges. This article must therefore be hereby marked "*advertisement*" in accordance with 18 U.S.C. Section 1734 solely to indicate this fact.

¶ To whom correspondence should be addressed. Tel.: 44-161-2004186; Fax: 44-161-2360409; E-mail: a.kitmitto@umist.ac.uk.

[1] The abbreviations used are: VGCCs, voltage-gated calcium channels; WGA, wheat germ agglutinin; HPLC, high pressure liquid chromatography; Ab, antibody; CHAPS, 3-[(cholamidopropyl)dimethylammonio]-1-propanesulfonate); RyR, ryanodine receptors; FSC, Fourier shell correlation.

external medium by two finger-like protrusions, extensions from the arches that curl around on each side. The dimensions and gross structural features of the dimeric particles are in good agreement with earlier rotary-shadowed images of freeze-dried, purified rabbit skeletal muscle VGCC complexes (20). Projection structures of negatively (uranyl acetate) stained monomeric VGCC complexes ~20 × 10 × 9 nm in size have also been reported (21). The monomers have the same height as the dimeric VGCC three-dimensional particles and are approximately half the base length. Serysheva *et al.* (22) studied VGCC complexes that differed somewhat in dimensions to the monomers reported in Ref. 21 but closely resembled the subcomplexes composed only of the α1 and β polypeptides, also described in Ref. 21. Recently, Wolf *et al.* (23) have presented a three-dimensional structure of a monomeric skeletal muscle VGCC using cryo-EM techniques. This structure shows some of the features reported by Murata *et al.* (21) but differs with that reported in Ref. 22. However, many of the features of the three-dimensional monomeric structure in Ref. 23 are also found in the dimeric structure presented here and earlier (19). The skeletal muscle monomers are approximately half the size of the dimer along one dimension, with the protruding "leg" density (23) bearing a strong resemblance to the "finger" domains that we have described.

We have now extended our studies to the cardiac muscle VGCC, which represents a much more challenging target for structural studies because of its naturally low abundance in the heart. Several groups (*e.g.* Refs. 24 and 25) have reported purification protocols for isolating the cardiac VGCC with some success, although there has been a lack of consistency in polypeptide composition. We describe here the first three-dimensional structure for the purified cardiac VGCC using the angular reconstitution technique that is based on the common lines theorem (26, 27) and using the EMAN image processing suite (28).

EXPERIMENTAL PROCEDURES

Purification of the Cardiac VGCC

Sarcolemmal membranes were prepared from bovine heart according to Ref. 29. All buffers throughout the purification were supplemented with a protease inhibitor mixture containing 0.1 mM phenylmethylsulfonyl fluoride, 1 mM benzamidine, 1 μM pepstatin A, and 1 μM L-*trans*-epoxysuccinyl-leucylamide(4-guananido)butane. Typically, 200 g of minced heart were used for one preparation. VGCCs were solubilized from the sarcolemmal membranes by incubation with 1% (w/v) digitonin (detergent:protein, 5:1) in 20 mM Tris, pH 7.5, for 45 min with gentle agitation at 4 °C and at a protein concentration of 2 mg/ml. Unsolubilized material was removed by ultracentrifugation at 50,000 × *g*. The supernatant was incubated on a DEAE column (10 ml, DEAE-Sepharose Fast Flow, Amersham Biosciences) equilibrated in solubilization buffer for 30 min. The column was washed with 5 column volumes of 20 mM Tris, pH 7.5, 2 mM $CaCl_2$ containing 0.1% (w/v) digitonin. The VGCCs were eluted from the column using a linear NaCl gradient (0–0.5 M). The fractions containing the cardiac VGCC were determined by immunoblotting with antibodies against α1, β, and α2 subunits. Monoclonal antibodies for the α1 and α2 subunits were purchased from Sigma, and the β polyclonal antibody prepared as described previously (13). The semi-purified VGCC fractions were pooled and incubated on a wheat germ agglutinin (WGA) column, 10 ml (Sigma), equilibrated with 20 mM Tris, pH 7.5, 2 mM $CaCl_2$, 0.1 M NaCl, 0.1% (w/v) digitonin for 30 min at 4 °C. The WGA column was washed with 5 column volumes of the equilibrating buffer and the cardiac VGCC eluted by the inclusion of 0.2 M *N*-acetylglucosamine (Sigma) in the equilibration buffer. The eluted fractions containing the cardiac VGCC (confirmed by immunoblotting) were concentrated using an Amicon concentrator (Millipore Ltd.). The concentrated fraction was then layered on top of a 5–30% (w/v) sucrose gradient in 20 mM Tris, pH 7.5, 2 mM $CaCl_2$, 0.1% (w/v) digitonin. Gradients were centrifuged for 90 min at 210,000 × *g*. 0.5-ml aliquots were taken from the gradient, with the presence of the cardiac VGCC complex in each fraction detected by Western blotting as described above. By using an Amicon concentrator, the buffer was exchanged (to remove the high concentrations of sucrose) with the purified cardiac VGCC material in a final buffer composed of 20 mM Tris, pH 7.5, 2 mM $CaCl_2$, and 0.1% (w/v) digitonin (including the protease inhibitor mixture). This method typically yielded between 20 and 40 μg/ml purified cardiac VGCC (~10–20 μg of purified protein/200 g of heart ventricles).

Gel Electrophoresis

Purified cardiac VGCC preparations were examined by SDS-PAGE. Aliquots were incubated with sample buffer (60 mM Tris (pH 6.8), 25% (v/v) glycerol, 2% (w/v) SDS, 14.4 mM 2-mercaptoethanol, 40 mM dithiothreitol, and 1% (w/v) bromphenol blue) at 90 °C for 5 min. Non-reducing sample buffer was made as above, but the dithiothreitol was omitted from the sample buffer mix. 4–20% gradient gels (Bio-Rad) were run at 200 V for 45 min. Native gels were run as described previously (19).

Immunoblotting

Protein bands from gels were transferred to nitrocellulose using a Biometra Electrophoretic transfer cell. Ponceau S staining (0.2% (w/v) Ponceau S, 3% (v/v) trichloroacetic acid, 3% (v/v) sulfosalicylic acid) of the nitrocellulose indicated that 90 min at 20 V was required for protein transfer as described previously (19). Monoclonal antibodies against the cardiac VGCC α1 and α2 subunits were purchased from Sigma, and antisera and affinity-purified antibodies raised against anti-β peptide (Ab2491) were prepared as described previously (19, 30).

Photoaffinity Labeling of the Cardiac VGCC Complexes

Covalent incorporation of [^{3}H]azidopine with purified cardiac VGCC was carried out as described previously (31), with some modifications. In brief, 40-μl aliquots (~30 μg/ml) were incubated in the dark with [^{3}H]azidopine with increasing concentrations ranging from 10 pM to 500 nM for 2 h on ice. The radioactive ligand was cross-linked to the cardiac VGCC samples by irradiation with a UV source (handheld Mineral light lamp, model UVSL-25) on ice for 5 min. Free azidopine was removed by running samples on gels after incubation with an equal volume of sample buffer. Gels were fixed and then soaked in Amplify™ (Amersham Biosciences) and exposed to Kodak film (Biomax Light Film) for up to 28 days at −80 °C. Gels were also run in parallel, from which the region corresponding to the α1 polypeptide was excised and incubated for 3 days with scintillation fluid prior to liquid scintillation counting (Packard 2000CA liquid scintillator). Radioactive counts (counts/min) were plotted against [^{3}H]azidopine concentration, and a double-reciprocal plot allowed an estimation of K_d.

Size-exclusion Chromatography

Size-exclusion chromatography was carried out by using a Bio-Rad HPLC system, equipped with a Bio-Gel TSK40 (300 × 7.5 mm) gel filtration column. Bio-Rad gel filtration standards, thyroglobulin (670 kDa), bovine γ-globulin (158 kDa), chicken ovalbumin (44 kDa), equine myoglobulin (17 kDa), and vitamin B_{12} (1.35 kDa), were used together with blue dextran (2 MDa, Sigma) and bovine serum albumin (64.43 kDa, Sigma) to calibrate the column. The column was equilibrated with 40 mM Tris (pH 7.5) and 0.5% (w/v) CHAPS in the absence of asolecithin. The approximate molecular masses of eluted protein were determined from a calibration curve constructed from elution volumes of the gel filtration standards. Affinity-purified antibody raised against anti-β peptide (Ab2491) was used to detect the presence of the skeletal muscle VGCC complexes in the various HPLC fractions. 10-μl aliquots from HPLC fractions were dotted onto nitrocellulose and left to dry at room temperature. The nitrocellulose was then incubated for 1 h with the primary antibody Ab2491 (dilution 1:200). An anti-rabbit IgG secondary antibody (Sigma) with an alkaline-phosphatase conjugate was employed for immunodetection. The spot areas were quantified using ImageQuant (version 5.1) after background subtraction.

Electron Microscopy

Cardiac VGCC preparations (20–40 μg/ml) were negatively stained with uranyl acetate and examined in a Philips Tecnai 10 transmission electron microscope as described previously (19). Electron micrographs were recorded at a calibrated magnification of ×43,400 on Kodak Electron Image film SO-163. Electron micrographs were digitized (UMAX PowerLook 3000 Scanner) at a scan step of 16 μm (3.7 Å/pixel at the specimen level). Samples of skeletal muscle VGCC at 100 μg/ml protein (in a buffer containing 20 mM Tris, pH 7.5, 0.5% (w/v) CHAPS (Sigma), 0.25% (w/v) asolecithin (L-α-phosphatidylcholine from soyabean, type II-S, Sigma), including protease inhibitors) were suspended in a thin layer of 5% (w/v) ammonium molybdate and 1% (w/v) trehalose, pH 7.0, as described in Ref. 32 on carbon-coated grids.

Lectin and Immunolabeling of Skeletal Muscle VGCC

Lectin, wheat germ agglutinin (WGA) (from *Triticum vulgaris*), conjugated to 5 nm colloidal gold (British Biocell Ltd.) was incubated with the purified skeletal muscle VGCC samples as described previously (19); samples were then stained with ammonium molybdate/trehalose as described above. VGCC complexes were also double-labeled with both WGA-gold and affinity-purified anti-β peptide antibody (Ab2491) (30). Samples were initially incubated with the WGA-gold conjugates (5 nm) followed by a second incubation with anti-β peptide antibody (Ab2491) each for 1 h at 4 °C followed by staining with ammonium molybdate/trehalose as described above.

Image Processing

Three-dimensional Reconstruction of the VGCCs—1,450 individual images were interactively selected from scanned micrographs of purified cardiac VGCC into 96 × 96 pixel boxes using the graphical interface boxer, part of the EMAN processing software (28). The selected particles were bandpass filtered, centered, and a set of reference-free class averages generated. In a similar manner 1,458 images of the purified skeletal muscle VGCC embedded in ammonium molybdate/trehalose were selected and treated using the same protocols for the cardiac VGCC data set. Following established procedures in the EMAN software suite, a preliminary three-dimensional model was determined from class averages that represented distinct views for each data set. The relative orientations of the characteristic views were determined using a Fourier common-lines routine and the averages combined to generate the preliminary three-dimensional model, the starting point for the main refinement loop. The class averages generated in the refinement loop are produced by a projection matching routine, whereby projections with uniformly distributed orientations of the preliminary three-dimensional model are used as references for classification of the raw data set, with the class averages from this step used to construct a new three-dimensional model. This is an iterative procedure with convergence assessed by examining the Fourier shell correlation (FSC) of the three-dimensional models generated from each iteration. The final three-dimensional volumes for the cardiac and skeletal muscle VGCC data sets were determined after eight rounds of iterative refinement, from 75 and 79 class averages, respectively. As a validation of the software, raw particles forming several of the major classes were selected in SPIDER and subjected to reference-free alignment. The resulting class averages were compared with the EMAN class average that demonstrated good agreement (data not shown). The three-dimensional reconstruction for each data set was carried out with 2-fold rotational (C2) symmetry imposed in accordance with previous analyses (19) and biochemical data.

The untilted data set (2,405 particles) of purified skeletal muscle VGCC complexes stained in uranyl acetate (19) was converted to EMAN format and a final three-dimensional model calculated as above.

Back projections of the three-dimensional volumes were generated using SPIDER commands (18). The resolution of each reconstruction was assessed by dividing the data set into two, calculating volumes for the two sub-sets, and estimated by the FSC coefficient with the resolution limit taken to be where the FSC value fell below 0.5 (33).

Two-dimensional Alignment of Lectin-labeled Skeletal Muscle VGCCs—SPIDER & WEB image processing packages (18) were employed for single particle analysis of WGA-gold single labeled VGCC complexes. Complexes were selected (n = 67) using a box size of 110 × 110 pixels. Particles were initially aligned using reference-free methods, with selected class averages from this procedure used for multireference alignment of the data set.

Modeling

Sequence alignment of the voltage-dependent potassium channel from the archaebacteria *Aeropyrum pernix* (KvAP) structure (34) with the cardiac and skeletal α1 subunits was done using ClustalW (35). Modeling of the KvAP structure (Protein Data Bank file 1ORQ) with the VGCC three-dimensional structures reported here was carried out using XtalView (36). Density maps were displayed using XtalView and also the SPOCK molecular graphics software (37).

RESULTS

Characterization of Purified Cardiac VGCC—A silver-stained SDS-PAGE gel of cardiac VGCC purified from beef heart is shown in Fig. 1*A, lane 2*, illustrating that the cardiac VGCC preparation is composed of four principal polypeptides, α1 (~230 kDa), α2 (~120 kDa), β (~66 kDa), and δ (~33 kDa).

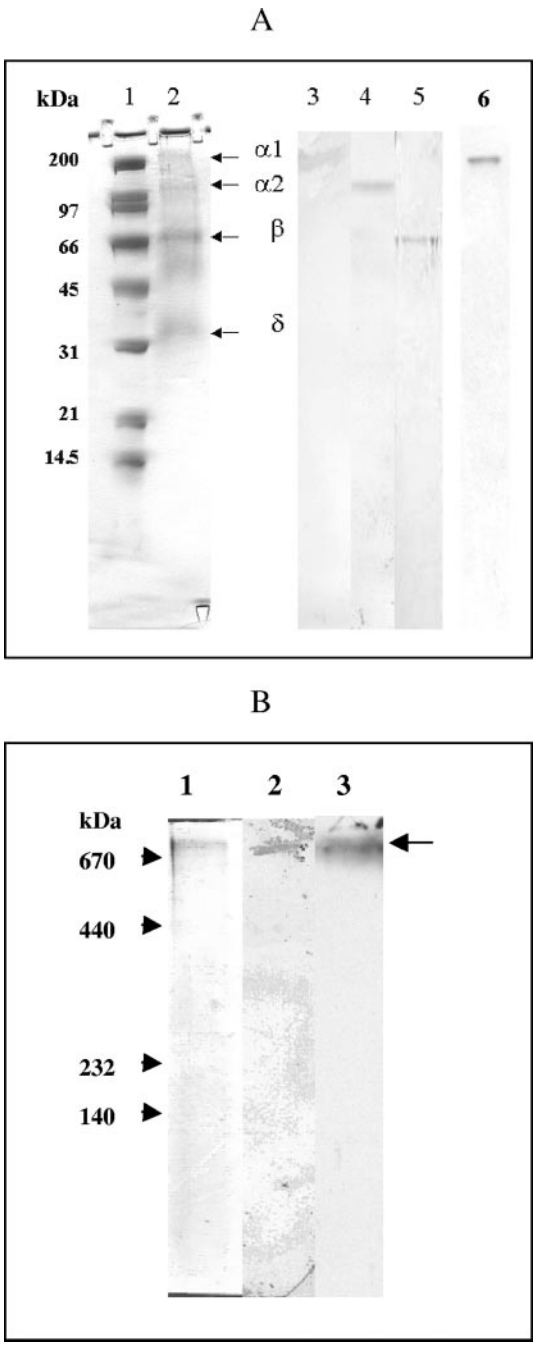

FIG. 1. **Characterization of the cardiac VGCC.** *A*, silver-stained SDS-PAGE gel of purified cardiac VGCC. *Lane 1*, molecular weight markers; *lane 2*, polypeptide profile of purified and reduced cardiac VGCC with major bands corresponding to the α1, α2, β, and δ subunits. Immunolabeling with antibodies against the following: *lane 3*, anti-α1; *lane 4*, anti-α2; and *lane 5*, anti-β. *Lane 6*, fluorogram of purified cardiac VGCC photoaffinity labeled with [^{3}H]azidopine showing specific incorporation into the α1 polypeptide. *B*, *lane 1*, native gel of purified cardiac VGCC showing a silver-stained band at ~800 kDa; *lane 2*, immunoblot with anti-α2 antibody showing labeling of the ~800-kDa band; *lane 3*, fluorogram of purified cardiac VGCC photoaffinity labeled with [^{3}H]azidopine showing specific incorporation into the ~800-kDa band.

Western blotting (*lanes 3–5*) confirmed the assignment of the α1, α2, and β subunits. The smeared band at ~50 kDa was also found in lanes containing no protein, suggesting this was an artifact. Photolabeling of the purified cardiac VGCC with [^{3}H]azidopine demonstrated that the radiolabeled ligand is specifically incorporated into a single band at ~230 kDa, corresponding to the α1 polypeptide (see fluorogram profile in *lane 6*). Further analysis of the purified channel by native gel elec-

trophoresis (Fig. 1*B, lane 1*) revealed that the cardiac VGCC migrates as a single high molecular weight species, ~800 kDa in molecular mass (indicated by the *black arrow*). The identity of the ~800-kDa band as cardiac VGCC was established by Western blotting with an anti-α2 antibody as shown in *lane 2*, and by photoaffinity labeling with [^{3}H]azidopine, see *lane 3*. The affinity of the cardiac VGCC (WGA eluent) for azidopine was examined by photolabeling with a range of [^{3}H]azidopine concentrations from 10 pM to 500 nM. Bands corresponding to the ~230-kDa α1 polypeptide from duplicate gels were excised and counted for radioactivity according to Ref. 38. A Lineweaver-Burk plot of [^{3}H]azidopine concentration against radioactive counts (counts/min) gave an estimated binding constant, K_d ~310 pM in agreement with Ref. 38 (data not shown). Analysis of the labeled material from the sucrose gradient indicated (assuming a 1:1 stoichiometric association of the azidopine and cardiac VGCC) that the purification protocol yielded samples ~86% pure cardiac VGCC.

Three-dimensional Structure of the Cardiac Muscle VGCC—A montage of selected areas from four electron micrographs of purified cardiac VGCC is shown in Fig. 2*A* after staining with uranyl acetate. The specimen is characterized by protein complexes ~20 nm in length (indicated by *black arrows*), highly reminiscent of the dimeric skeletal VGCC complexes reported earlier (19). However, unlike the skeletal muscle VGCC, which presented a preferred orientation of the complex in uranyl acetate, several different views of the cardiac VGCC were identified as shown in Fig. 2*B* (*1st* and *2nd rows*). The presence of multiple orientations for the cardiac VGCC allowed us to calculate a three-dimensional structure using common lines methodology (26, 27) with the EMAN software (28). Examples of some class averages, from the range of orientations used to determine a preliminary three-dimensional model, are shown in Fig. 2*B, 2nd row*, with an aligned particle representative of each group in the row above. Back projections of the final three-dimensional channel volume (Fig. 2*B, 3rd row*) showed good correlation to the class averages and the raw data.

The three-dimensional volume of the cardiac VGCC, at ~2.5 nm resolution (estimated on the basis of FSC = 0.5 (33)), is displayed in Fig. 3, after 2-fold rotational symmetry was applied. 2-Fold rotational (C2) symmetry was assigned on the basis of the biochemical data and by comparison with the dimeric skeletal muscle VGCC in Ref. 19. Presented in *A–D* are orthogonal side views revealing a complex ~19 nm in height, *i.e.* ~2 nm less than the skeletal muscle form (19). The overall shape of the cardiac VGCC as displayed in *A* and *C* is less rounded than the skeletal muscle VGCC (19) with a distinct tapering toward one end of the complex. By using wire-frame contouring to display the volume (see Fig. 3*C*), the finger domain and the outer band of density formed by the two monomer arches, structural features previously reported for the skeletal muscle dimeric structure in Ref. 19, are clearly apparent. The finger domains are protein densities protruding from the monomer arches that surround a central aqueous compartment (see Fig. 3*G*). Rotation of the view in Fig. 3, *A* and *C,* around the C2 axis by 90° presents a view of one of the monomer arches, which can be seen to be resolved into 3 domains and has a distinct kink in the middle. On either side of the monomer arch there is a finger domain, giving a total complex width of ~14.5 nm, as shown in Fig. 3, *B* and *D*. In this orientation the cardiac VGCC can also be found to narrow toward the top end of the complex, a feature we term the "nose." The nose region at the top of the complex is shown in more detail in Fig. 3*E* and is found to be formed by the intimate association of the monomer arches creating a narrow bridge, with some contribution from the tips of the finger domains. The opposing face of the complex (*bottom*) of the structure (Fig. 3*F*) is characterized by two distinct protein domains in the center of the complex with the monomer arches curling around on either side. The interior of the complex is revealed in Fig. 3*G* with the foremost portion of the complex (~6 nm) cut away to reveal a central chamber that encloses a volume with a height and width ~5 × 3 nm, respectively, and depth of ~4 nm (as outlined by the *black dotted line*).

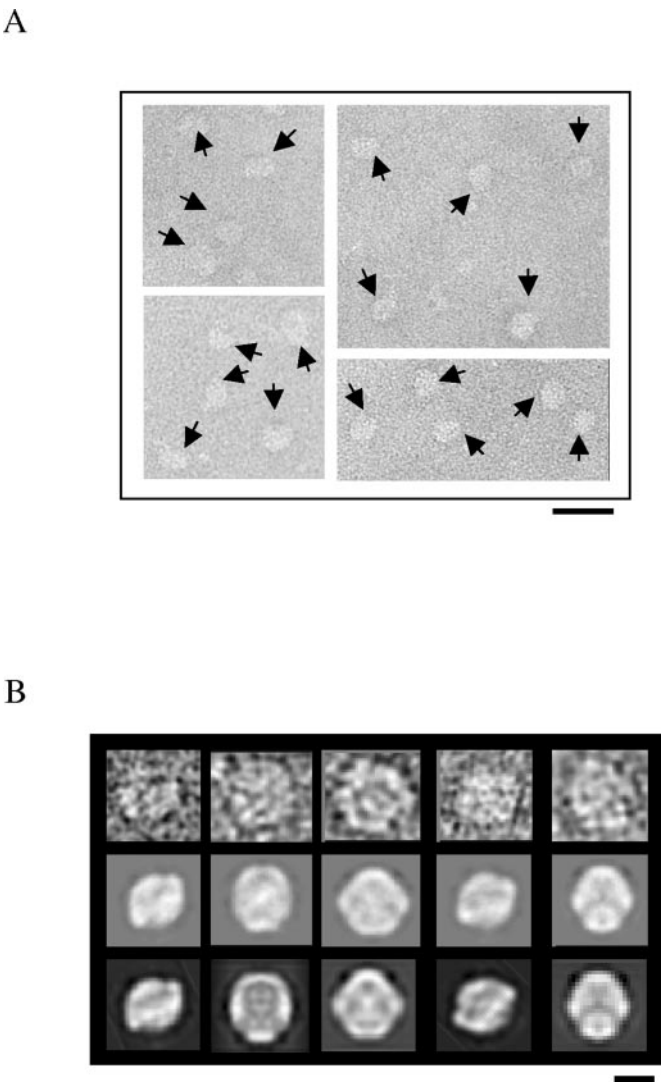

FIG. 2. **Electron micrographs of negatively stained cardiac VGCC and data from image processing.** *A*, areas from four different electron micrographs showing purified cardiac VGCC complexes negatively stained with uranyl acetate. *Scale bar*, 40 nm. *B*, *1st row* shows examples of raw images in different orientations, with the respective two-dimensional class averages in the *2nd row*. *3rd row* shows back projections of the three-dimensional cardiac VGCC structure showing good correlation to the corresponding class averages. *Scale bar*, 10 nm.

Comparison of the Cardiac and Skeletal Muscle VGCC Structures—In view of the greater number of projection classes for the cardiac VGCC, thus resulting in a greater sampling of three-dimensional space, the skeletal muscle VGCC structure described in Ref. 19 is inevitably less detailed by comparison, especially along the direction perpendicular to the main projection due to the missing cone phenomenon (39). We also tested whether differences could arise because of different image processing procedures. The data set used for the skeletal muscle VGCC was therefore reanalyzed using the common lines approach. By using the EMAN software (28), several views of the complex in addition to the predominating side

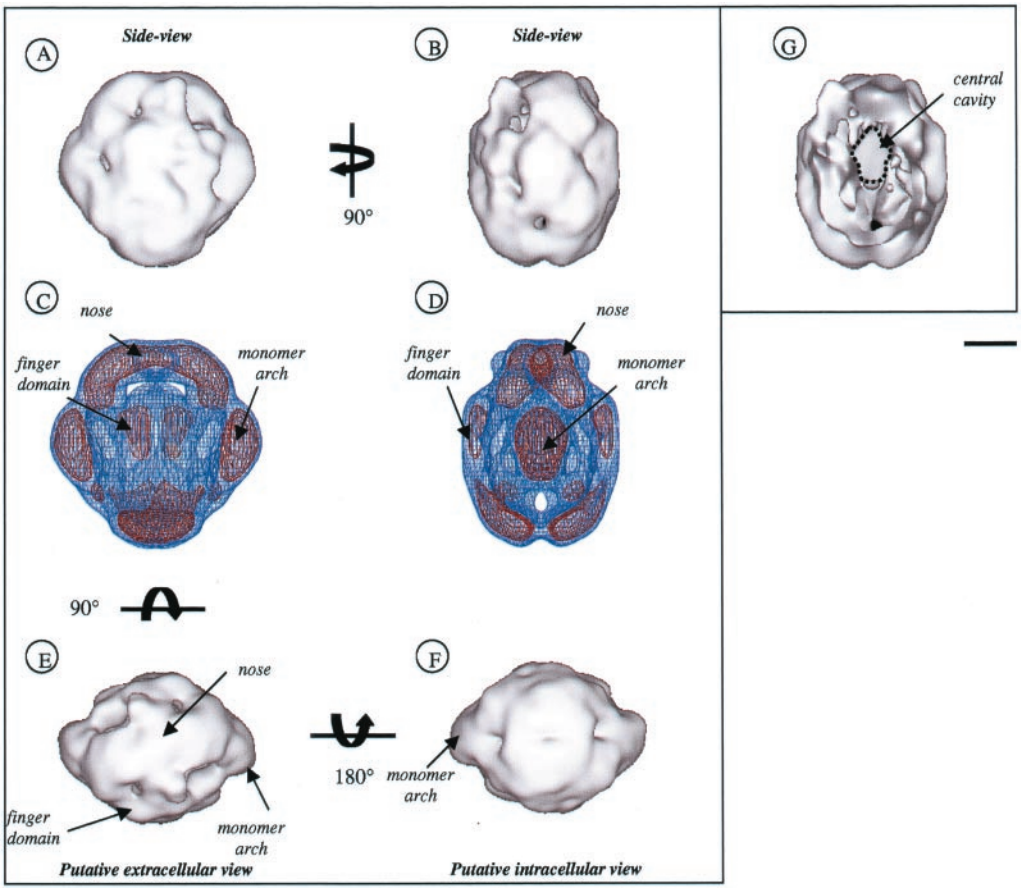

FIG. 3. **Three-dimensional structure of the cardiac VGCC.** *A*, surface representation of the cardiac VGCC as viewed parallel to the membrane plane (displayed at 2σ above the mean density). *B*, rotation of image in *A* around the 2-fold rotational symmetry (C2) axis by 90°. *C* and *D*, three-dimensional structures as presented in *A* and *B*, respectively, but displayed using contouring (*blue mesh* = 2σ and *red mesh* = 3.5σ above the mean density). *E*, putative extracellular view of the complex, and *F*, putative intracellular view of the cardiac VGCC. *G*, cut-away of the three-dimensional structure as displayed in *B* to reveal the interior of the cardiac VGCC structure. *Scale bar*, 5 nm.

view, a structure circular in shape with a diameter of ~22 nm, were identified permitting the calculation of a new three-dimensional volume (Fig. 4), at an estimated resolution of ~2.7 nm. As can be observed in Fig. 4, the resulting structure was consistent with the structure obtained by the random conical-tilt methodology with the monomer arches and finger domains readily identifiable. The more rounded appearance of the skeletal muscle VGCC (diameter ~23 nm) in comparison to the cardiac version, when viewed from the side (*i.e.* spanning the membrane), is also discernible (compare Fig. 3*A* with Fig. 4*A*). Rotation of the view in Fig. 4*A* around the C2 axis by 90° shows a monomer arch flanked by two finger domains giving a total complex width of ~17 nm, some ~3 nm wider than that reported earlier (19). The central aqueous chamber is also revealed (Fig. 4*C*) and has a diameter of ~7 nm, similar in size to that described previously (19) but larger and more spherical in appearance than that formed by the cardiac VGCC dimer (Fig. 3*G*). The nose domain is well defined in Fig. 4. This feature was not previously resolved (19) but can be seen here to be composed of two protein densities, arranged in a similar manner to that observed in the cardiac VGCC three-dimensional structure.

For immunolabeling and lectin-gold labeling studies to probe the quaternary organization of multisubunit protein complexes, it is preferable to use a stain that more faithfully preserves weak non-covalent interactions at neutral pH. For this purpose ammonium molybdate with trehalose produces a stable embedding medium at pH 7 (32). Inclusion of trehalose has been reported to reduce flattening, lead to greater orientational freedom, and provides electron beam protection to protein complexes in the high vacuum (32). We have therefore employed this medium for labeling skeletal muscle VGCC with the aim of assigning the extracellular and intracellular sides of the complex (see later). A further advantage, when examining skeletal muscle VGCCs embedded in ammonium molybdate/trehalose (same batch as characterized in Ref. 19), was the increased number of orientations of the VGCC dimers observed, when compared with uranyl acetate-stained samples. A representative electron micrograph of purified skeletal muscle VGCC complexes after staining with ammonium molybdate/trehalose is shown in Fig. 5*A*. The VGCC complexes were found to be very similar in size to those reported previously (19) (*black arrows*) except that the central cavity often appeared to be less well contrasted. Examples of class averages displaying different orientations of the skeletal muscle VGCC are shown in Fig. 5*B*, *2nd row*, with representative particles from each class average presented in the row above. Back projections of the three-dimensional volume are shown in the *3rd row* and demonstrate good correlation with the class averages and raw data. The three-dimensional volume is displayed at two different thresholds using wire-frame contouring in Fig. 6. Fig. 6*A* shows the side view of the skeletal muscle VGCC (comparable with Fig. 3*A* and Fig. 4*A*). The overall rounded appearance (diameter ~23.5 nm) is again confirmed, and the finger domains, monomer arches, and nose feature are resolved (see Fig. 6, *A* and *B*). The top and bottom of the complex are presented in Fig. 6, *C* and *D*, respectively. The bottom view is characterized by two juxtaposed protein domains, and the top view

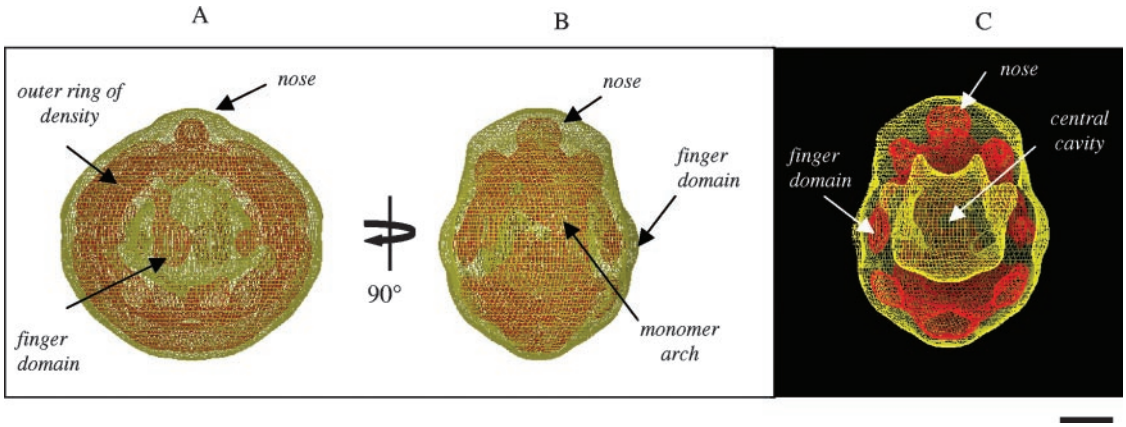

FIG. 4. **Three-dimensional structure of the skeletal muscle VGCC negatively stained with uranyl acetate displayed at two different density thresholds (*yellow mesh* = 2σ and *red mesh* = 5σ above the mean density).** *A*, side view (parallel to the membrane plane) of the skeletal muscle VGCC three-dimensional structure. *B*, rotation of the view in *A* by 90° around the C2 axis revealing the nose domain. *C*, same view as in *B* with the foremost portion of the complex cut away to display the central aqueous chamber. *Scale bar*, 5 nm.

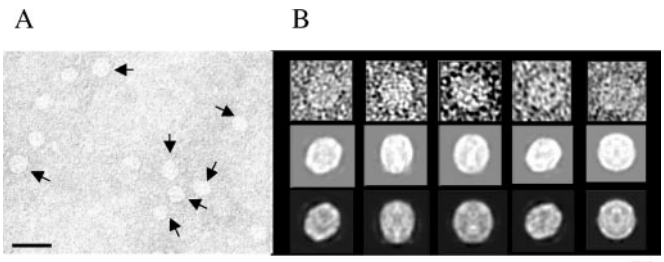

FIG. 5. **An electron micrograph of skeletal muscle VGCC negatively stained with ammonium molybdate/trehalose and data from image processing.** *A*, field of negatively stained (ammonium molybdate/trehalose) skeletal muscle VGCC complexes. *Scale bar*, 50 nm. *B*, *1st row* shows examples of raw images in different orientations with the corresponding two-dimensional class averages in *2nd row*. *3rd row* shows back projections of the three-dimensional skeletal muscle VGCC structure showing good correlation to the corresponding class averages. *Scale bar*, 10 nm.

shows the nose to be formed by a ridge of density as also observed for the cardiac VGCC structure in Fig. 3. In Fig. 6*E,* the front portion of the complex (when orientated as in *B*) has been cut away to reveal a large central cavity, with a height of ~8 nm and width of ~4 nm, narrowing toward the bottom. It is difficult to estimate the depth of the cavity as it was found not to be a continuous void but a series of interconnecting chambers (data not shown).

Labeling of the Skeletal Muscle VGCC—By having established the reproducibility of the structural analysis in ammonium molybdate/trehalose, we undertook antibody and WGA-gold labeling of the skeletal muscle receptor to map the approximate positions of the β polypeptides and the extracellular glycosylated moieties, respectively. Fig. 7*A*, *left panel*, shows an example of a VGCC complex dual labeled with an anti-β subunit IgG and WGA-gold conjugate, whereas the particle in the *right panel* is an example of a dimer labeled with two WGA-gold conjugates and a single anti-β IgG. No VGCC complexes were observed with two IgG molecules bound. Fig. 7*B* is a diagrammatic representation of dual-labeling results, indicating the relative binding positions of the WGA-gold conjugates and the anti-β IgG for 20 VGCC complexes. The *open circles* represent the gold spheres of the WGA-gold conjugate, and the *gray arrows* represent the approximate positions of the anti-β IgG. From these data it is apparent that the WGA-gold conjugates cluster at two locations that appear to be symmetry-related on the upper portion of the complex, whereas the anti-β IgG molecules bind to the lower portion close to the C2 symmetry axis and on the opposite side of the complex to the WGA-gold.

Single particle averaging of VGCC complexes labeled with one WGA-gold conjugate was carried out in order to obtain a more precise localization of the glycosylation site(s) on the extracellular face of the complex, as shown in Fig. 7*C*. The averaged projection is consistent with previous projections generated from larger numbers of unlabeled particles, presenting a side view of the complex. The *dotted white line* indicates the position of the C2 symmetry axis. The gold label is visualized as an electron dense (*black*) circular domain ~5 nm in diameter which is slightly offset to the right of the dyad axis and close to the nose feature protruding from the tapered end of the complex. The gold sphere is located ~4 nm away from the VGCC complex with the gap consistent with the presence of the intervening lectin molecule (~36 kDa).

Skeletal Muscle VGCC Monomers and Dimers—Purified skeletal muscle VGCC, previously that ran as a single band on a native gel (19), was applied to a size-exclusion chromatography column (in the absence of lipids). Two principal peaks, I and II, eluting at 15.40 and 19.83 min, respectively, were observed (Fig. 8) with protein levels in the ratio of peak I:peak II = 1:2.5 (data not shown). Both peaks were immunoreactive to the anti-β peptide antibody, Ab2491 (Fig. 8*A*), and SDS-PAGE gave typical polypeptide profiles for VGCC (data not shown). Calibration of the size-exclusion column showed that the two peaks corresponded to ~1.07 MDa and ~480 kDa which would correlate to the expected masses of a VGCC dimer and monomer, respectively. Peak I eluted later than the void volume (blue dextran eluted at 13.93 min), and so it was unlikely that peak I represented randomly aggregated VGCC complexes. Aliquots from peaks I and II were examined by electron microscopy after staining with ammonium molybdate/trehalose. In peak I ellipsoidal particles ~20 nm in length were observed (Fig. 8*B*, *top row*) that were indistinguishable from the skeletal VGCC dimers reported earlier (19) and described here. Examination of peak II found protein particles approximately half the size (diameter ~10 nm) of those in peak I (compare Fig. 8*B*, *top* and *bottom rows*). These smaller particles were similar in shape and size to the monomeric VGCC complexes assigned as "face-on" views reported by Murata and colleagues (21), and to orientations of the three-dimensional structure more recently described by Wolf *et al.* (23).

DISCUSSION

Oligomeric Form of L-type Voltage-gated Calcium Channels—The structural and biochemical data presented here for the purified bovine cardiac VGCC reveal that it has been isolated as a stable dimer with an approximate molecular mass of

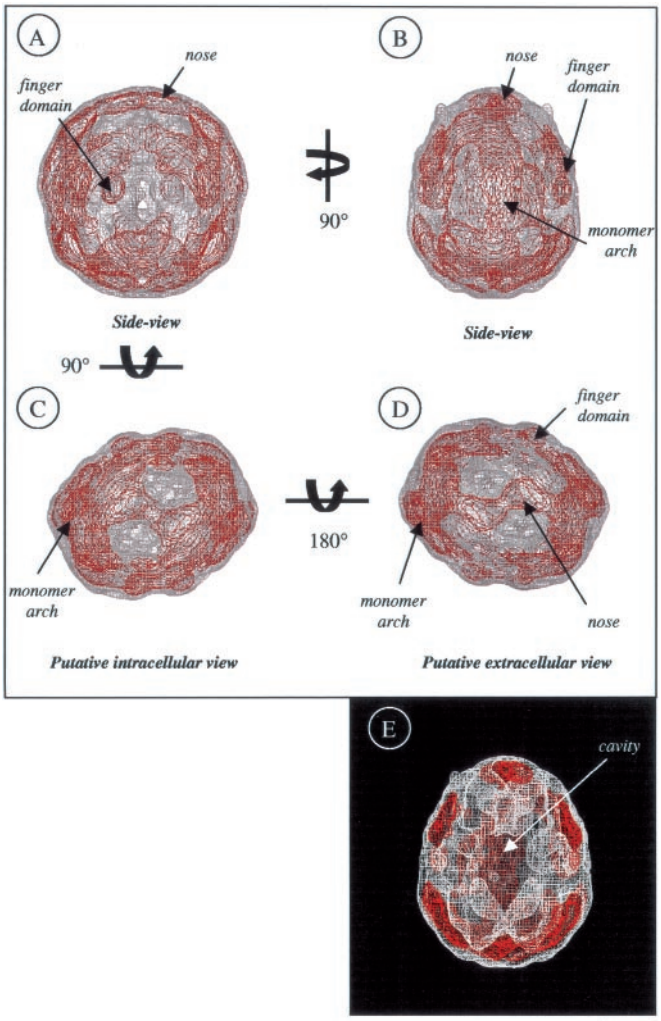

FIG. 6. **Three-dimensional structure of the skeletal muscle VGCC embedded in ammonium molybdate/trehalose displayed at two different density thresholds (*silver mesh* = 2σ, *red mesh* = 3.5σ, above the mean density).** *A*, side view of the skeletal muscle VGCC as viewed parallel to the membrane plane. *B*, rotation of image in *A* around the C2 axis by 90°, *C*, putative intracellular view of the complex; *D*, putative intracellular view of the skeletal muscle VGCC. *E*, cut-away of the three-dimensional structure as orientated in *B* to reveal the interior cavities. *Scale bar*, 5 nm.

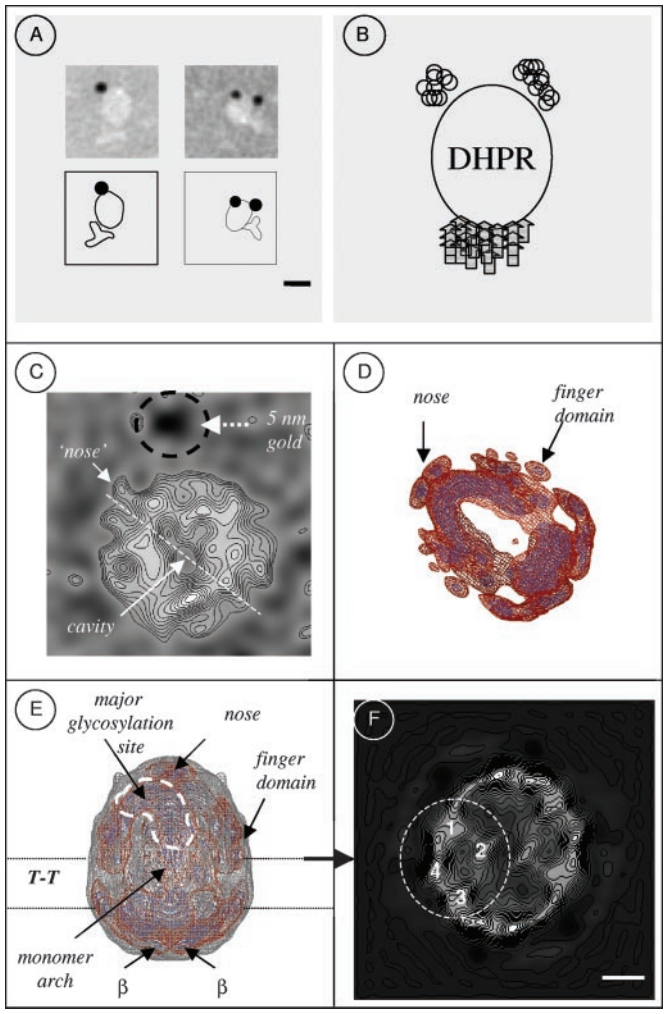

FIG. 7. **Lectin (WGA) and immunolabeling (anti-β IgG) of purified dimeric skeletal muscle VGCC complexes (ammonium molybdate/trehalose staining).** *A*, *left panel* shows an example of a dual-labeled dimeric VGCC complex decorated with a single WGA-gold conjugate and a single anti-β antibody. The *right panel* shows an example of a tri-labeled dimeric VGCC complex with two WGA-gold conjugates and a single anti-β IgG bound. *Scale bar*, 10 nm. *B*, diagrammatic representation of the VGCC dimer complex showing the approximate binding positions of the WGA-gold conjugate and anti-β IgG for 20 dual-labeled VGCC dimers. *Arrows* represent position of the IgGs (center of *arrow* approximates to the intersect of the Y shape of the IgG molecules); *open circles* represent the position of the WGA-gold conjugates. *C*, projection map of WGA-gold labeled skeletal muscle VGCC dimers. *D*, three-dimensional structure of the skeletal muscle VGCC (stained with ammonium molybdate/trehalose) displayed using two different density thresholds (contouring; *red mesh* 3.5σ and blue mesh 4.5σ above the mean density) orientated so to illustrate correlation of the nose domain with the projection map in *C*. *E*, putative orientation of the skeletal muscle VGCC three-dimensional structure with respect to the t-tubular (*T*-*T*) membrane. *F*, slice through the three-dimensional skeletal muscle VGCC dimer at the putative transmembrane/extracellular interface. Slices taken perpendicular to the C2 axis. *Scale bar*, 10 nm.

~800 kDa, consistent with our previous studies of a dimeric form of the skeletal muscle VGCC (19). The purified dimeric cardiac VGCC complex binds [^{3}H]azidopine, and this ligand is specifically associated with the α1 polypeptide. These data demonstrate that the cardiac dimeric form is functional in terms of drug binding with a K_d value for azidopine in agreement with findings published previously (38). The data presented in Fig. 8 show that the skeletal muscle VGCC dimer may be dissociated to monomers under conditions employed for size-exclusion chromatography, *i.e.* high detergent:protein ratio, dilution, extended run times, and absence of lipid. Native gels of purified VGCC complexes run at low temperatures and higher protein concentrations displayed only one principal band at ~750 kDa (19) and one corresponding immunoreactive band, demonstrating that the VGCC was stable under mild electrophoretic conditions. A comparison of the results from native gels, EM, and the size-exclusion chromatography data reported here suggests that different procedures employed for chromatography led to the dissociation of dimers to monomers. This dissociation may be associated with the presence or absence of lipids (20) during purification that could indicate lipid mediation of the oligomeric form of VGCC. On comparing the purification methods used by various groups, it can be seen that those methods leading to the isolation of skeletal muscle VGCC monomers employed digitonin for solubilization, whereas that leading to dimers used CHAPS/asolecithin (19). The rotary shadowed particles with dimensions and structural features very similar to the dimeric VGCC, which were reported by Leung *et al.* (20), also involved the use of CHAPS/asolecithin for isolation of the skeletal muscle form. Other differences between the preparations may arise from alternative purification procedures. In this study we followed an es-

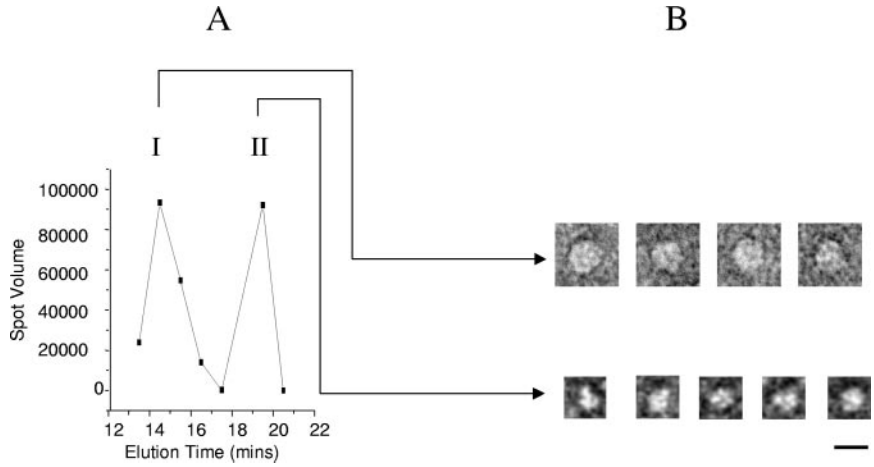

FIG. 8. **Dissociation of skeletal muscle VGCC dimers to monomers.** Dot blot analysis of eluted purified VGCC from the size-exclusion column. Spots were digitized and quantified using ImageQuant (version 5.1) and volumes (after background subtraction) plotted against eluted fractions. *A*, negatively stained (ammonium molybdate/trehalose) VGCC dimers eluting in HPLC peak I. *B*, negatively stained (ammonium molybdate/trehalose) VGCC monomers eluting in HPLC peak II. *Scale bar*, 20 nm.

tablished four-step method (40), whereas Murata *et al.* (21) employed a three-step procedure, Serysheva *et al.* (22) employed a rapid two-step isolation protocol, with Wolf *et al.* (23) following a procedure similar to this group with the main difference being the detergent employed.

Here we also describe the isolation of a dimeric cardiac VGCC that has been solubilized from the sarcolemmal membranes using digitonin, but with no supplemental lipids added. This suggests that for the cardiac VGCC dimer factors other than exogenous lipid are important for dimer stabilization. Differences in lipid composition between the skeletal muscle transverse-tubules and sarcolemmal membranes and the differential solubilizing effects of the digitonin on skeletal and cardiac forms of VGCC may be pertinent. For example, we do observe a partial dissociation of the cardiac VGCC dimers to monomers when samples of purified material are diluted (~1:2) with buffer (data not shown). A possible explanation may be that sufficient endogenous lipids co-purify with the cardiac channel to stabilize dimer formation but when diluted concentrations are no longer sufficient to help maintain the oligomeric form.

As yet it remains to be established whether the monomeric, dimeric, or an even higher oligomeric form is the functional unit of the skeletal or cardiac VGCCs. However, the concept of oligomeric forms of skeletal and cardiac VGCCs have been described by other groups, *e.g.* Chang and Hosey (41) in which it was demonstrated that the skeletal muscle VGCC can be isolated as a single high molecular weight species (~800–900 kDa). Furthermore, functional reconstitution experiments by Hymel *et al.* (42) also indicated an oligomerization of the skeletal muscle VGCC. More recently, Marks and co-workers (43) have isolated oligomers of the cardiac ryanodine receptors tetramers (RyR2). Reconstitution of the coupled RyR2 into planar lipid bilayers showed the oligomers to be functional with the multiple channels showing simultaneous gating. Similar data were also reported previously (43) for the skeletal muscle isoform (RyR1). This may be important for understanding skeletal muscle excitation-contraction coupling for which a direct association of the VGCCs and RyRs is indicated. Clearly a priority for future work will now be establishing whether the dimer formation is a result of detergent-induced oligomerization or if they represent a functional form. Investigations will include reconstitution experiments of the dimeric VGCC complexes, described here, into lipid bilayers to determine whether they are functional and, if they are, whether the gating of the two channels is synchronized.

Comparison of the Cardiac and Skeletal Muscle VGCC Dimer Three-dimensional Structures—A comparison of the cardiac and skeletal muscle VGCC volumes presented in Figs. 3, 4, and 6 finds that they share a common architectural design with one of the characteristic features being a central aqueous compartment formed by the two halves of the dimers. It seems unlikely that the central compartment would penetrate the lipid bilayer, indicating that the complex is probably asymmetric with respect to the membrane, in agreement with topological predictions. However, the more complex nature of the interconnecting chambers forming a central aqueous region in the three-dimensional structure of the skeletal muscle VGCC after embedding with ammonium molybdate/trehalose reflects the different behavior of the negatively charged molybdate ions compared with the positively charged uranyl ions. Therefore, in order to gain a more detailed definition of the interior compartment(s) formed by the two halves of the VGCC dimers, future work will concentrate on examining unstained specimens. However, by using negative stains we are able to conclude that since the stain penetrates the cavity, it must be at least partially accessible from the external medium, and close examination of the three-dimensional VGCC volumes find that in all structures the outer surfaces are punctated by small holes that run through to the central chamber. The three-dimensional structure of the voltage-gated sodium channel (44) also describes a series of orifices that connect through to several central chambers suggesting that ion permeation may be a common facet important to function. However, whether the narrow entrances through the finger domains confer any selectivity for Ca^{2+} ions remains to be investigated.

Labeling data of the skeletal muscle VGCC with both anti-β IgGs and lectin-gold are consistent with the dimeric nature of the ellipsoidal ~20 nm particles and also support topology predictions and biochemical data (13, 45, 46) that place the $\alpha 2$ and β polypeptides on the opposite faces of the VGCC complexes. By using single particle analysis methods, we have also demonstrated that the WGA-gold binds close to the nose feature, and correlation of this structure to the skeletal muscle three-dimensional volume (see Fig. 7*D*) has permitted assignment of the extracellular face of the complex, placing the β subunits on the opposite face, on the intracellular side of the complex. We have therefore tentatively assigned the intracellular and extracellular faces of the VGCC complex allowing orientation of the skeletal muscle form with respect to the transverse-tubular membrane as shown in Fig. 7*E*.

The putative intracellular face is characterized by two densities closely associated at the dyad axis, related by rotational symmetry (*e.g.* see Fig. 3*F*). Therefore, we have tentatively assigned these protein domains as slices through the β subunits in accordance with labeling described here. The organization of the β polypeptides in this manner may explain why no dimeric skeletal muscle VGCC complexes were observed la-

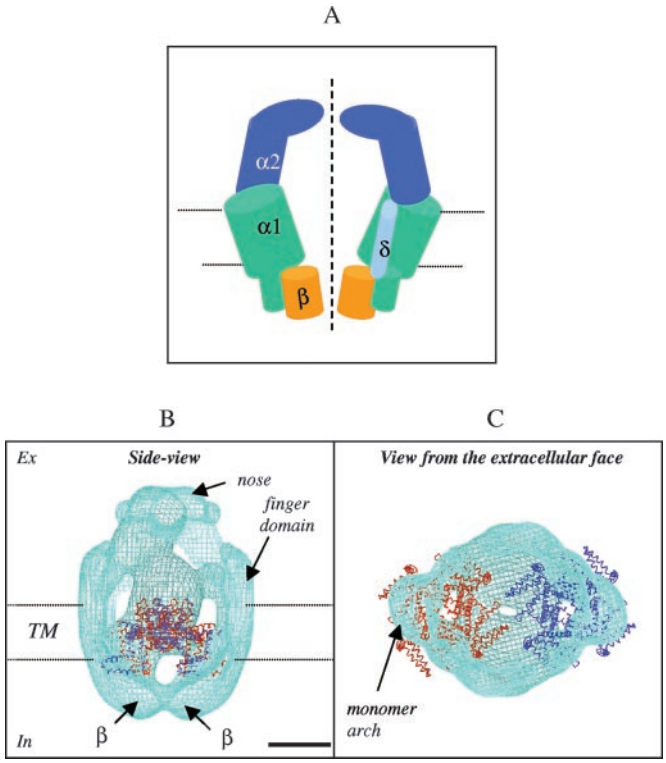

FIG. 9. **Three-dimensional structure of the cardiac muscle VGCC orientated with respect to the lipid bilayer, with modeling of the two KvAP tetramers in the putative position of the α1C polypeptides.** *A*, schematic representation of the cardiac muscle VGCC dimer illustrating the proposed subunit organization. *Dotted lines* indicate putative position of the transmembrane (*TM*) region. *B*, cut-away of a side view of the cardiac VGCC displayed using contouring (*turquoise mesh* = 3σ), the two KvAP tetramers are colored *red* and *blue*. *C*, as viewed from the putative extracellular face and slabbed to the predicted extracellular/transmembrane interface to reveal the arrangement of the KvAP tetramers. *Scale bar*, 10 nm.

beled with two anti-β IgGs since steric hindrance would prevent such an association. Because the α2 polypeptide forms much of the extracellular mass of the VGCCs (13, 45), it seems reasonable to infer that the nose and finger domains are mainly formed by the α2 subunits. Correlation of the nose feature of the cardiac VGCC three-dimensional reconstruction with the skeletal muscle structure also permits assignment of the intracellular and extracellular faces of the cardiac complex as shown in Fig. 9. Statistical analyses of the orientation of the cardiac VGCC with respect to the skeletal muscle channel structure using cross-correlation methods support our interpretation of the data. Cross-correlation of the cardiac VGCC with the skeletal muscle volume after rotation of the cardiac structure, so that the nose features of the cardiac and skeletal VGCCs are positioned 180° with respect to each other, found a significant drop (0.11) in the cross-correlation coefficient.

Differences between the three-dimensional structures of the VGCC dimers are apparent, however, when viewed from the side (compare Figs. 3*A* with 4*A* and 6A) in which the cardiac complex has a more tapered appearance. As discussed in the Introduction, the cardiac VGCC is believed to lack a γ subunit, and the SDS-PAGE data presented here support that conclusion. Because the γ subunit is believed to be a membrane protein (11), then it should be localized to the region assigned to the lipid bilayer. The absence of the γ subunit in the cardiac VGCC complex might therefore account for its more tapered appearance. We also observed that the quaternary organization of the cardiac VGCC dimer leads to a smaller structure than the skeletal muscle VGCC complex by at least 2 nm in each dimension, notwithstanding factors such as variations in stain distribution, a different detergent annulus, and reconstructive methods. Although the total mass of the complexes will be similar, we suggest that the absence of the two γ subunits has led to a closer association of the cardiac VGCC monomers, as also indicated by a smaller central cavity. Similarly, the absence of the γ polypeptides in the cardiac VGCC dimer assembly has resulted in differences to the overall shape of the intracellular and extracellular faces in comparison to the skeletal muscle form, as well as to the region assigned to the lipid bilayer as discussed above. However, we can conclude that the organization and protein-protein contacts between the α1, α2δ, and β polypeptides are preserved between the two VGCCs from different tissue types, with the data presented here revealing a common architectural design. In addition, we can surmise that the γ polypeptides are not necessary for dimer contacts. Cross-linking experiments should be helpful for future investigations of the subunit associations in the dimer complexes. Presented in Fig. 9*A* is a schematic representation of the cardiac VGCC three-dimensional structure, consistent with the structural data presented here.

Structural Comparison of Other Existing Models for the Skeletal Muscle VGCCs—Two other three-dimensional structures of a monomeric skeletal muscle VGCC have been reported (22, 23). Paradoxically, neither of these structures shows close resemblance to each other. This may be, in part, attributable to a variation in purification protocols as discussed above and the resolutions of the final three-dimensional volumes. Some similarity is seen between the two-dimensional projection images of negatively stained monomeric skeletal muscle VGCCs presented by Murata and co-workers (21) and with certain orientations of the three-dimensional structure described by Wolf *et al.* (23). However, Murata *et al.* (21) provided a different interpretation of their data, suggesting an asymmetric distribution of the protein densities across the transverse-tubular membrane, with a large extracellular mass, in agreement with the analyses of the dimeric structures presented here. On close examination of the monomeric structure of the skeletal muscle VGCC from Wolf *et al.* (23), structural features consistent with the dimeric VGCC volumes are apparent. For example, the finger domains reported here seem to correlate well to the "leg" density in the monomer protruding from a large globular domain, including assignment of these densities by both groups as the α2 polypeptide. However, we have interpreted our data so that the outer ring of density (which would correspond to the large globular domain of the monomer) is orientated so that it spans the membrane, *i.e.* orthogonal to that shown in Wolf *et al.* (23), but in agreement with Murata *et al.* (21). It is interesting to note that reorientation of the Wolf *et al.* (23) monomer structure in agreement with our interpretation of the dimer structures would still result in the leg domain residing on the extracellular side but would also lead to the hydrophilic β subunit being localized to the intracellular side of the t-tubular membrane, in the cytosol, which would be more in-line with topological predictions that the β subunit is a soluble protein. Unexpectedly, the pseudo 4-fold symmetry of the α1 subunit is not discernible in either of the monomeric three-dimensional structures of the skeletal muscle VGCC reported previously (22, 23). However, the pseudo 4-fold symmetry of the comparative polypeptide forming the voltage-gated sodium channel was observed in the EM-derived three-dimensional structure (44) at similar resolutions. As described here, our interpretation of the dimeric VGCCs structure places the α2 polypeptide partially above the α1 subunit on the extracellular face, and this would obscure a pseudo 4-fold symmetry of the α1. Presented in Fig. 7*F* is a slice through the skeletal muscle VGCC

dimer complex (perpendicular to the C2 axis) at the putative interface of the transmembrane/extracellular region, as depicted in Fig. 7*E*. This projection map shows that the dimer, at the interface, is characterized by a pair of rectangular-shaped domains, ~11 × 8.5 nm (enclosed by the *white dashed circle*) composed of four densities numbered 1–4 in the figure. The four protein densities surround a central low density region, ~1.8 × 4.0 nm in agreement with the organization that has been reported for the voltage-gated sodium (44) and potassium channels (47) and is consistent with the concept of the four transmembrane segments of the α1 polypeptide arranged pseudo-symmetrically to form a central pore.

Modeling of the Tetrameric Voltage-dependent Potassium Channel with the Cardiac VGCC Dimer—Recently, MacKinnon and co-workers (34) reported the structure of the tetrameric voltage-dependent potassium channel from *A. pernix* (KvAP) by x-ray crystallography at 3.2 Å. Sequence alignment of the KvAP monomer with the cardiac and skeletal VGCCs, α1C and α1S polypeptides, found homology of the potassium channel monomer with the second transmembrane domain of both the α1C and α1S subunits, showing significant conservation of the transmembrane helices, in particular IIS4. As such it seemed reasonable to model two KvAP tetramers with the cardiac muscle VGCC dimer, displayed at high thresholds to show only the principal protein densities, in the region we have tentatively assigned as transmembrane, see Fig. 9, *B* and *C*. Fig. 9*B* presents a side orientation of the cardiac VGCC dimer with the foremost portion of the structure slabbed to reveal a possible organization of the two KvAP tetramers, which when modeled in this way contribute toward the densities we have termed "monomer arches." Fig. 9*C* shows the structure as viewed from the extracellular face looking down on the 2-fold rotational axis, with the extracellular portion of the complex cut away to reveal the putative transmembrane/extracellular interface illustrating that the two KvAP tetramers can be readily accommodated in the cardiac three-dimensional structure. An unusual and unexpected feature of the reported crystal structure of KvAP was the organization of the S3–S4 helices into a paddle formation leading to a new proposal for gating charged movements. These paddles are suggested to "flip" from the intracellular side of the membrane to a transmembrane orientation in response to membrane depolarization. More recently, alternative models for the organization of the helices forming the S3–S4 paddles in the KvAP crystal structure have been suggested (48, 49), placing the S1 and S2 helices at the periphery of the channel, S4 adjacent to S5 with S3 not undergoing the transmembrane motion as described by MacKinnon and co-workers (34). The organization of a KvAP monomer described previously (48) would lead to a more compact KvAP tetrameric structure, two of which would also be comfortably housed within the molecular envelope of the dimeric VGCC structures presented here.

Future work is now aimed at higher resolution studies by cryo-electron microscopy methods coupled with reconstitution to determine the physiological viability of the novel dimeric forms of the cardiac and skeletal muscle VGCCs reported here.

Acknowledgments—We thank Alhaji Bukar Khamis (University of Manchester Institute of Science and Technology) and Professor Alan Eddy (University of Manchester Institute of Science and Technology) for useful discussions and Dr. Anthony Davies (University College London) for a critical review of the manuscript. This work was supported in part by an equipment grant from the Wellcome Trust.

REFERENCES

1. Tanabe, T., Takeshima, H., Mikami, A., Flockerzi, V., Takahashi, H., Kangawa, K., Kojima, M., Matsuo, H., Hirose, T., and Numa, S. (1987) *Nature* **328,** 313–318
2. McCleskey, E. W., and Almers, W. (1985) *Proc. Natl. Acad. Sci. U. S. A.* **82,** 7149–7153
3. Mikami, A., Imoto, K., Tanabe, T., Niidome, T., Mori, Y., Takeshima, H., Narumiya, S., and Numa, S. (1989) *Nature* **340,** 230–233
4. Leung, A. T., Imagawa, T., and Campbell, K. P. (1987) *J. Biol. Chem.* **262,** 7943–7946
5. Striessnig, J. (1999) *Cell. Physiol. Biochem.* **9,** 242–269
6. Barclay, J., Balaguero, N., Mione, M., Ackerman, S. L., Letts, V. A., Brodbeck, J., Canti, C., Meir, A., Page, K. M., Kusumi, K., Perez-Reyes, E., Lander, E. S., Frankel, W. N., Gardiner, R. M., Dolphin, A. C., and Rees, M. (2001) *J. Neurosci.* **21,** 6095–6104
7. Ellis, S. B., Williams, M. E., Ways, N. R., Brenner, R., Sharp, A. H., Leung, A. T., Campbell, K. P., McKenna, E., Koch, W. J., Hui, A., Schwartz, A., and Harpold, M. M. (1988) *Science* **241,** 1661–1664
8. De Jongh, K. S., Warner, C., and Catterall, W. A. (1990) *J. Biol. Chem.* **265,** 14738–14741
9. Hullin, R., Friedrich, I., Khan, Y., Wirtz, S., Mohacsi, P., Varadi, G., Schwartz, A., and Herzig, S. (2003) *J. Biol. Chem.* **278,** 21623–21630
10. Pichler, M., Cassidy, T. N., Reimer, D., Haase, H., Krause, R., Ostler, D., and Striessnig, J. (1997) *J. Biol. Chem.* **272,** 13877–13882
11. Jay, S. D., Ellis, S. B., McCue, A. F., Williams, M. E., Vedvick, T. S., Harpold, M. M., and Campbell, K. P. (1990) *Science* **248,** 490–492
12. Letts, V. A., Felix, R., Biddlecome, G. H., Arikkath, J., Mahaffey, C. L., Valenzuela, A., Bartlett, F. S., Mori, Y., Campbell, K. P., and Frankel, W. N. (1998) *Nat. Genet.* **19,** 340–347
13. Brickley, K., Campbell, V., Berrow, N., Leach, R., Norman, R. I., Wray, D., Dolphin, A. C., and Baldwin, S. A. (1995) *FEBS Lett.* **364,** 129–133
14. DeWaard, M., Scott, V. E. S., Pragnell, M., and Campbell, K. P. (1996) *FEBS Lett.* **380,** 272–276
15. Brice, N. L., Berrow, N. S., Campbell, V., Page, K. M., Brickley, K., Tedder, I., and Dolphin, A. C. (1997) *Eur. J. Neurosci.* **9,** 749–759
16. Gurnett, C. A., Felix, R., and Campbell, K. P. (1997) *J. Biol. Chem.* **272,** 18508–18512
17. Gao, T. Y., Chien, A. J., and Hosey, M. M. (1999) *J. Biol. Chem.* **274,** 2137–2144
18. Frank, J., Radermacher, M., Penczek, P., Zhu, J., Li, Y. H., Ladjadj, M., and Leith, A. (1996) *J. Struct. Biol.* **116,** 190–199
19. Wang, M.-C., Velarde, G., Ford, R. C., Berrow, N. S., Dolphin, A. C., and Kitmitto, A. (2002) *J. Mol. Biol.* **323,** 85–98
20. Leung, A. T., Imagawa, T., Block, B., Franziniarmstrong, C., and Campbell, K. P. (1988) *J. Biol. Chem.* **263,** 994–1001
21. Murata, K., Odahara, N., Kuniyasu, A., Sato, Y., Nakayama, H., and Nagayama, K. (2001) *Biochem. Biophys. Res. Commun.* **282,** 284–291
22. Serysheva, II, Ludtke, S. J., Baker, M. R., Chiu, W., and Hamilton, S. L. (2002) *Proc. Natl. Acad. Sci. U. S. A.* **99,** 10370–10375
23. Wolf, M., Eberhart, A., Glossmann, H., Striessnig, J., and Grigorieff, N. (2003) *J. Mol. Biol.* **332,** 171–182
24. Kuniyasu, A., Oka, K., Yamada, T. I., Hatanaka, Y., Abe, T., Nakayama, H., and Kanaoka, Y. (1992) *J. Biochem.* (*Tokyo*) **112,** 235–242
25. Haase, H., Striessnig, J., Holtzhauer, M., Vetter, R., and Glossmann, H. (1991) *Eur. J. Pharmacol. Mol. Pharmacol. Sec.* **207,** 51–59
26. Vanheel, M. (1987) *Ultramicroscopy* **21,** 111–123
27. Serysheva, II, Orlova, E. V., Chiu, W., Sherman, M. B., Hamilton, S. L., and Vanheel, M. (1995) *Nat. Struct. Biol.* **2,** 18–24
28. Ludtke, S. J., Baldwin, P. R., and Chiu, W. (1999) *J. Struct. Biol.* **128,** 82–97
29. Jones, L. R. (1988) *Methods Enzymol.* **157,** 85–91
30. Berrow, N., Tedder, I., Page, K., Brice, N., Amos, B., and Dolphin, A. C. (1995) *J. Physiol.* (*Lond.*) **489,** P52–P53
31. Taylor, A. M., Storm, J., Soceneantu, L., Linton, K. J., Gabriel, M., Martin, C., Woodhouse, J., Blott, E., Higgins, C. F., and Callaghan, R. (2001) *Br. J. Pharmacol.* **134,** 1609–1618
32. Harris, J. R., Hoeger, U., and Adrian, M. (2001) *Micron* **32,** 599–613
33. Bottcher, B., Wynne, S. A., and Crowther, R. A. (1997) *Nature* **386,** 88–91
34. Jiang, Y. X., Lee, A., Chen, J. Y., Ruta, V., Cadene, M., Chait, B. T., and MacKinnon, R. (2003) *Nature* **423,** 33–41
35. Thompson, J. D., Higgins, D. G., and Gibson, T. J. (1994) *Nucleic Acids Res.* **22,** 4673–4680
36. McRee, D. E. (1999) *J. Struct. Biol.* **125,** 156–165
37. Christopher, J. A., and Baldwin, T. O. (1998) *J. Mol. Graphics* **16,** 285–285
38. Ferry, D. R., Rombusch, M., Goll, A., and Glossmann, H. (1984) *FEBS Lett.* **169,** 112–118
39. Penczek, P., Radermacher, M., and Frank, J. (1992) *Ultramicroscopy* **40,** 33–53
40. Curtis, B. M., and Catterall, W. A. (1984) *Biochemistry* **23,** 2113–2118
41. Chang, C. F., and Hosey, M. M. (1990) *Biochem. Biophys. Res. Commun.* **172,** 751–758
42. Hymel, L., Striessnig, J., Glossmann, H., and Schindler, H. (1988) *Proc. Natl. Acad. Sci. U. S. A.* **85,** 4290–4294
43. Marx, S. O., Ondrias, K., and Marks, A. R. (1998) *Science* **281,** 818–821
44. Sato, C., Ueno, Y., Asai, K., Takahashi, K., Sato, M., Engel, A., and Fujiyoshi, Y. (2001) *Nature* **409,** 1047–1051
45. Jay, S. D., Sharp, A. H., Kahl, S. D., Vedvick, T. S., Harpold, M. M., and Campbell, K. P. (1991) *J. Biol. Chem.* **266,** 3287–3293
46. Ruth, P., Rohrkasten, A., Biel, M., Bosse, E., Regulla, S., Meyer, H. E., Flockerzi, V., and Hofmann, F. (1989) *Science* **245,** 1115–1118
47. Sokolova, O., Kolmakova-Partensky, L., and Grigorieff, N. (2001) *Structure* **9,** 215–220
48. Gandhi, C. S., Clark, E., Loots, E., Pralle, A., and Issacoff, E. Y. (2003) *Neuron* **40,** 515–525
49. Lee, H. C., Wang, J. M., and Swartz, K. J. (2003) *Neuron* **40,** 527–536